Fingering instability in combustion: An extended view

Ory Zik and Elisha Moses
Department of Physics of Complex Systems, The Weizmann Institute of Science, Rehovot 76100, Israel
(Received 29 October 1998)

We detail the experimental situation concerning the fingering instability that occurs when a solid fuel is forced to burn against a horizontal oxidizing wind. The instability appears when the Rayleigh number for convection is below criticality. The focus is on the developed fingering state. We present direct measurements of the depletion of oxygen by the front as well as new results that connect heat losses to the characteristic scale of the instability. In addition, we detail the experimental system, elaborate (qualitatively and quantitatively) on the results that were previously presented, and discuss new observations. We also show that the same phenomenological model applies to electrochemical deposition. [S1063-651X(99)05007-2]

PACS number(s): 47.20.Ma, 82.40.Py, 47.20.Hw

I. INTRODUCTION

We all encounter and use combustion on a daily basis, from the lighting of a match to the engine of a car. Still, we maintain a primal fascination with flames, exemplified by the dancing motion of a bonfire. This has origins that go beyond the complexity and beauty of the phenomenon itself, ''where you have such beauty and brightness as nothing but combustion or flame can produce''[1]. Fortunately, perhaps, our understanding of the flame is still poor, leaving that mysterious fascination intact [1].

We turn instead to forms of combustion in which the complicated nonequilibrium chemical process can be restrained and controlled, aiming for an accuracy that is comparable to the degree of control of more conventional front propagation systems. A flame is fundamentally determined by the availability of fuel, oxidant, and heat, and its dynamics can be localized to the region of interaction. This realization leads us to the study of the combustion front, and to limit it to a slow burning regime. We can further simplify the dynamics by the use of a thin gap (Hele-Shaw) geometry, which provides a crucial constraint and subsequent simplification.

We have recently shown that a thin solid, burning against an oxidant wind, develops a steady fingering state [2]. Conceptually the effect is like a ''print-out'' of the thermal diffusion instability. It appears in a well defined regime of the Rayleigh and Péclet numbers (below the threshold of vertical convection and with prevailing molecular diffusion in the horizontal plane). The characteristic length (finger width) is determined by the ability of the front to release heat, while the distance between fingers is determined by the availability of oxygen. The quality of experimental control reveals a new state which has an applicational significance; a sole finger of fire can slowly propagate in an oxygen-rich environment, remaining below the threshold of conventional detection. The current paper elaborates on the experimental and phenomenological findings as well as presenting new results.

Interfacial instabilities have been extensively studied in simpler, less reactive, growth systems [3–7]. The pattern is typically characterized by one length scale—the fastest growing wavelength in the linear spectrum [8]. Notable examples are solidification [9], nematic-isotropic transition in liquid crystals [10], and viscous fronts [11]. These systems are usually treated within the framework of the Stefan problem, where the front is a solution of one or more Laplacian fields (e.g., pressure or temperature) satisfying some boundary conditions on the interface. The characteristic scale is determined by various system properties, e.g., the gradient of the field that drives the instability (as in solidification [9] and liquid crystals [10]), the system scale (as in viscous fronts [7]), or the front velocity (as in eutectic growth [12]). In principle, more than one characteristic scale can be expected, depending on the number of fields that govern the front [13]. Our previous paper [2] described two decoupled length scales that correspond directly to the two different fields: the transport of reactants and transport of heat.

Previous works on combustion have already revealed a number of interfacial instabilities [14]. The most notable is the *thermal-diffusion* instability in ''premixed'' flames (i.e., the oxygen and ''fuel'' are mixed before burning). This instability has two fields, based on two competing transport processes [15]. The transport of reactants has a destabilizing effect, while the transport of heat has a stabilizing effect. To see this, consider a bump in the interface. It is protruding into a colder region of fresh oxygen. The higher availability of oxygen promotes the propagation of the bump, while the excessive heat losses impede it.

The thermal-diffusion instability was first reported in 1882 on a Bunsen burner [16] and has been extensively studied ever since [14]. The rich behavior exhibited by this system includes interesting modes like ''rotation'' and ''ratcheting'' [17]. Flame propagation over thin solid fuels has also been previously studied. The main focus was the flame spread rate [18–20]. A cellular structure observed in this system was recently related to the thermal-diffusion instability [21]. From the theoretical side, recent work predicts a connection between the Saffman-Taylor instability and two-dimensional filtration combustion [22] (see also Ref. [3] and references therein).

Our system combines the two-dimensional (2D) ''Hele-Shaw'' geometry [11] with combustion (not in a filtration regime). The measurements are performed in the comparatively slower and experimentally convenient combustion regime termed *smoldering* [23]. This is a nonflaming mode (i.e., the emitted gas does not ''glow'' in the visible light)

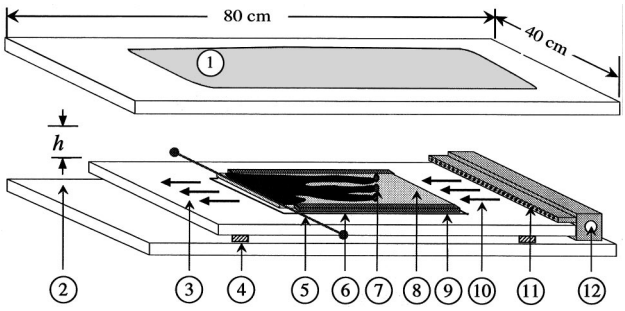

FIG. 1. Schematic representation of the setup. 1, glass top; 2, variable gap between top and bottom plates *h*; 3, outflow of combustion products; 4, spacers to control *h*; 5, ignition wire; 6, heat conducting boundaries; 7, flame front; 8, fuel; 9, interchangeable bottom plate; 10, uniform flow of O_2/N_2; 11, gas diffuser; 12, gas inlet.

where oxygen interacts with solid fuel to produce char, gaseous products and the heat that sustains the process. The oxidizing gas is supplied in a uniform flow, opposite to the direction of the front propagation (i.e., the fuel and oxygen are fed to the reaction from the same side). This configuration enhances the destabilizing effect of reactant transport, which plays the same role as in the thermal-diffusion instability. The reduction to two dimensions is critical in order to suppress the effect of convection and plumes near the front. Interestingly, a 3D version of our experiment has recently been conducted onboard the space shuttle [24]. A simple estimation of the Rayleigh number in our experiment shows the equivalence of quasi-2D and microgravity in neutralizing gravitational effects.

In this configuration the front exhibits a *directional fingering instability* with two decoupled length scales (the finger width and the spacing between fingers) [2]. The nondimensional control parameter is the Péclet number Pe which measures the relative importance of advection and molecular diffusion [25]. The instability appears below a critical value of Pe. The two length scales correspond directly to the two key transport mechanisms: transport of heat and transport of reactants. The distance between fingers is self-consistently determined by Pe. Although heat transport plays a key role in the instability, we show with a phenomenological model that reactant transport alone determines the front velocity and the spacing between fingers. The agreement between the model and measurements is remarkable (no free parameters). The behavior of the spacing between fingers is analogous to electrodeposition [26,27]. On the other hand, the characteristic scale (finger width) is effectively independent of Pe. We show that it depends on the ability of the front to release heat.

The origin of the instability should ultimately yield from a linear theory. At this stage such a theory is lacking and remains an open challenge. Our preliminary derivation of a Mullins-Sekerka type analysis shows that the main obstacle to deriving such a theory lies in translating the far-from-equilibrium moving flame front into an adequate boundary condition.

II. SETUP

The cell is shown schematically in Fig. 1. It has a tempered glass top for visualization (1 in Fig. 1). The spacing *h* between the sample plane and glass top is adjustable (2 and 4 in Fig. 1). The fuel is a rectangular sheet of dimensions $20\times 20\ \mathrm{cm}^2$ (8 in Fig. 1). Our ''fuel'' is mainly filter paper. However, the effect is fuel independent. It occurs in all the combustible materials that we examined, from standard stationery paper to polyethylene sheets (see Sec. VII). Our quantitative measurements were conducted on the paper produced by Whatman (mostly grade no. 2). Its main advantages are its uniformity and the available data on its properties. Another advantage of using this paper is the fact that it smolders at a relatively low temperature (about 600 °C), allowing us to work in small gap sizes (down to 0.2 cm) without cracking the glass.

The fuel sample is stretched on the bottom of the cell with uniform tension. The uniformity is achieved with a system of springs against which the paper is stretched. The uniform stretching is able to prevent the ''crumpling'' of the burned paper that can arise in some of the regimes. The springs are recessed into the bottom plate. The part of the bottom plate which touches the sample can be changed to allow a study of the effect of ambient heat conductivity (9 in Fig. 1). Aluminum adhesive strips are used to create uniform heat conductive lateral boundary conditions (6 in Fig. 1). These stripes are 0.025 cm higher than the sample. This serves to decrease the supply of oxygen from the sides of the sample. Without these boundary conditions, the propagation along the boundaries prevails and the front is not uniform.

The emphasis of the experimental design was as follows. (i) Creating a uniform 2D gas flow (10 in Fig. 1); (ii) Creating a uniform 1D ignition (5 in Fig. 1). The uniform flow was achieved with a gas diffuser consisting of an array of orifices which was designed to produce a laminar wind of oxygen and nitrogen (11 in Fig. 1). The diffuser consists of an array of 80 cylindrical holes of diameter 0.06 cm and length 0.8 cm. To avoid the inhomogeneities produced by the sides, we limited the experiment to the central part of the flow channel.

We used two other diffusers to check the influence on the results: a diffuser with a parabolic shape and a diffusing ''slot'' ($0.07\times 30\ \mathrm{cm}^2$). Both changed the flow slightly, but did not have any influence on the results. The parabolic diffuser was designed to produce a uniform hydrodynamical resistance (by varying both the length and the diameter of the holes).

We use two systems of rotatometers to control the fluxes of oxygen (F_{O_2}) and nitrogen (F_{N_2}) that are fed into the diffuser (12 in Fig. 1). The velocity is calculated as the flux divided by the effective system cross section, $V_{O_2,N_2}=F_{O_2,N_2}/S$ with $S=25\times \mathrm{h}\ \mathrm{cm}^2$. We used smoke visualization for calibration and independent measurements of the gas-flow velocity. The measured smoke velocities agree within $\pm 10\%$ with the calculated velocities. The uniformity of the flow was also verified with this technique (Fig. 2). The visualization agent was cigarette smoke. We pumped an N_2/O_2 mixture through a ''matrix'' of 12 cigarettes. More conventional smoke production methods (e.g., using resins, powders, or water vapors) did not work due to the small orifice dimensions of the diffusers.

Uniform ignition was achieved with a resistively heated

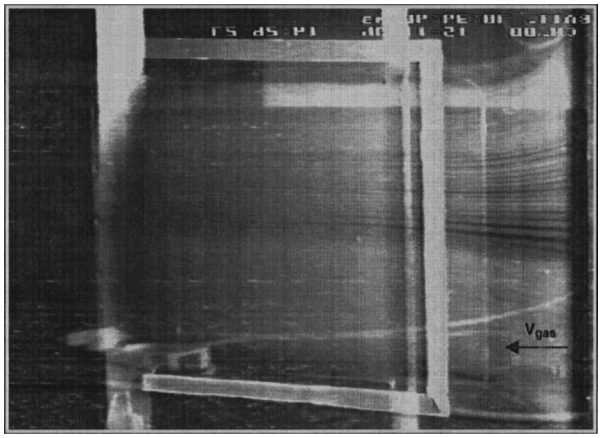

FIG. 2. Flow visualization with cigarette smoke is used to check the uniformity of the gas flow, as well as for an independent measurement of the gas velocity. The smoke flows from right to left. The rectangular frame marks the region where the sample is typically placed. The uniformity of the flow in this region is evident. The image was taken with reflected light.

thin ($R=55\ \mu$m) tungsten wire, which was placed along a line at the fuel edge (5 in Fig. 1). The ignition can be either in the downwind part of the sample (counterflow regime) or at the upwind part (coflow regime). The wire is recessed into the bottom plate so that it does not interfere with the flow. It has a spring to maintain tension as the wire undergoes thermal expansion. In Fig. 3 we show a time sequence that demonstrates the initial evolution of a fingering state, after the wire was heated. The arrow in the bottom picture marks the heated ignition wire. The initial nonuniformity in the ignition is erased as the front propagates.

Creating uniform ignition along the width of the sample is especially difficult near extinction ($V_{O_2}<1$ cm/s). We overcame this problem by coating the ignition zone with a saturated solution of nitrocellulose in acetone, letting the acetone evaporate and applying an initial pulse of oxygen at 12 cm/s. The evolution near extinction is shown in Fig. 4 (from bottom to top). The front is initially smooth due to the high flux of oxygen. The second picture from the bottom shows the

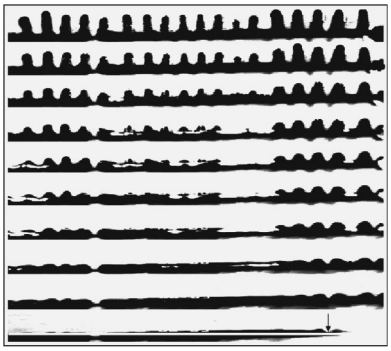

FIG. 3. A time sequence (the images are 1.2 s apart, time increases upwards) showing the initial evolution of the front after ignition, in the tip splitting regime. The sinusoidal pattern evolves soon after ignition. The peaks of the sine wave grow towards the oxygen source. The arrow in the bottom image marks the heated ignition wire. The initial small nonuniformity in the ignition is recovered by the pattern.

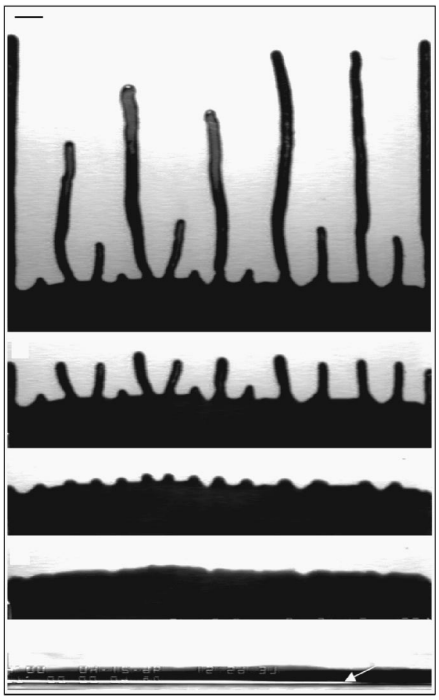

FIG. 4. Initial evolution near extinction. The sinusoidal perturbation appears immediately after we cut V_{O_2} (from 15 to 0.33 cm/s) and then develops into a steady state of sparse fingers. Times from ignition are (bottom to top) 1, 5.3, 8.6, 35.8, and 193.5 s.

sinusoidal pattern that develops after the supply of oxygen is cut. The steady state of sparse fingers (top) is achieved after a selection process. This has no effect on the front velocity (see the following).

A test for the experimental design [especially for points (i) and (ii) above] is that the growth will attain a steady state and will maintain it. Figure 5 shows the position as a function of time for various values of V_{O_2}. The system attains a steady state immediately after ignition. The front velocity (slope) remains unchanged throughout the run. Near extinction we see that the transition from the initial ''boost'' to the steady-state condition (shown in Fig. 4) has a short transient effect. The sharp transition (indicated by the arrow in Fig. 5) shows how the system immediately recovers to its steady state.

Following is the list of control parameters and the ranges that we covered.

(i) Gas flow velocity $V_{gas}(=V_{O_2}$ if $a=1$ and $V_{O_2+N_2}$ if $a\neq 1)$: $0-25\pm 0.2$ cm/s.

(ii) Relative N_2 content in the gas $a=f_{O_2}/(f_{O_2}+f_{N_2})$, where $f_{O_2,N_2}=F_{O_2,N_2}/S$: $0.6\leqslant a\leqslant 1$. (Note that as long as $a=1$, we will use $V_{O_2}=f_{O_2}$ for the specific oxygen flux.)

(iii) Gap between cell top and bottom h: $(0.2-1.4)\pm 0.04$ cm. (The small gap inhibits natural convection —an inexpensive alternative to turning off gravity.)

(iv) Fuel (composition, thickness, density, ash content).

(v) Heat conductivity of the bottom plate λ: $10^7\gtrsim\lambda\gtrsim 10^3$ ergs/cm s K.

Most of the experiments were performed with $a=1$, Whatman paper no. 2, $h=0.5$ cm, aluminum bottom plate ($\lambda=2.4\times 10^7$ erg/cm s K). The molecular diffusion coeffi-

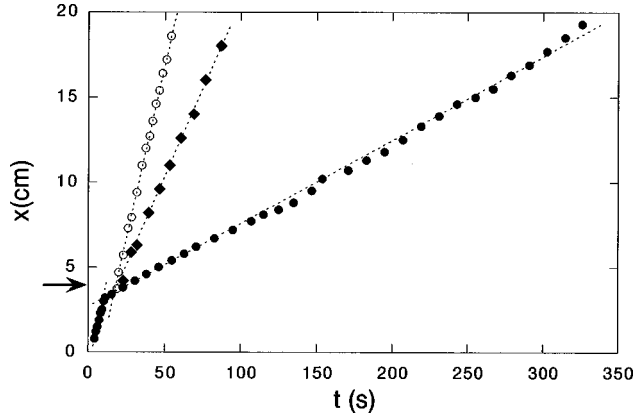

FIG. 5. Typical $x-t$ data for measurements of u. $V_{O_2}=8.6$ cm/s, empty circles (connected front, no fingering); $V_{O_2}=2$ cm/s, full circles (fingering and tip splitting); $V_{O_2}=0.2$ cm/s (verge of extinction, fingering, without tip splitting), full squares. The respective front velocities are $u=0.41$, 0.21, and 0.045 cm/s. The lines represent the linear fits from which the velocity is measured. The small arrow marks the point at which the transient (initial boost) of the propagation near extinction ($V_{O_2}=0.2$ cm/s) ends and the measurement begins (see Fig. 4). The transition from the ignition stage to the steady state is sharp. x is defined as the position of the foremost finger. Similar results are obtained when x is defined as the average finger position.

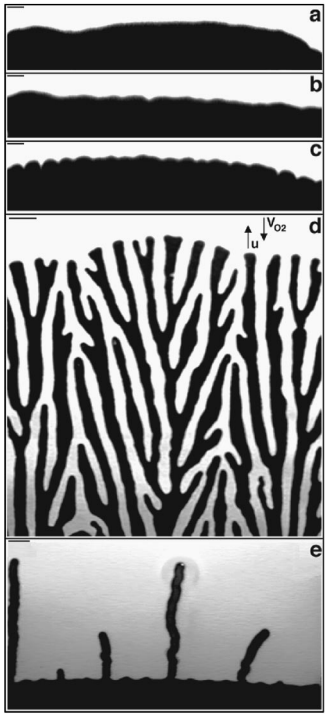

FIG. 6. Steady-state patterns in counterflow combustion of thin solid fuel as a function of oxygen flow V_{O_2} [decreasing from (a) to (e)]. (a) Stable front, (b) irregular front, (c) periodic pattern, (d) fingering pattern with tip splitting, (e) fingering without tip splitting. In all regimes, a bright spot (like the one at the tip of the central finger) typically appears just before the tip stops growing. The charred area (black) propagates from bottom to top. The fingering pattern defines two length scales: the finger width w and the spacing between fingers d. The scale bars are 1 cm. The gap between plates is $h=0.5$ cm. The oxygen flow velocity V_{O_2} is directed downwards and the front velocity u is directed upwards [arrows in (d)]. The values are (top to bottom) $V_{O_2}=11.4$, 10.2, 9.2, 1.3, 0.1 cm/s and $u=0.5$, 0.48, 0.41, 0.14, 0.035 ± 0.01 cm/s.

cient is taken to be $D=0.25$ cm^2/s. We ignore its temperature dependence.

The measured quantities are (with the typical systematic error) as follows.

(i) Front velocity u (±0.05 cm/s).

(ii) Finger width w (±0.05 cm).

(iii) Distance between fingers d (±0.05 cm).

(iv) Density, thickness, and composition of products.

(v) Oxygen content of the gaseous products ($\pm10\%$).

u, d, and w were measured through CCD images of the front (we used a Sony XC-75CE camera, peaks in the visible range, digitization matrix of 736×512, and with geometrical distortion less than 2%). The front velocity was measured with a code that we added to the software NIH Image 1.6 [28]. It automatically identifies the propagating front in predetermined steps. The accuracy in resolving the front is about five pixels. The composition of the solid products (char) was measured with gas chromatography [29]. The oxygen content was measured by an electrochemical sensor (we used ''Emproco'' 020697 with a typical response time of 5 s and probe diameter of 0.3 cm). The sensor is fed by a slow suction pump (at 0.1 LPM). The temperature of the front was measured to be $600\pm40\,^{\circ}$C (using a nitrogen cooled IR camera).

III. THEORETICAL AND PHENOMENOLOGICAL PICTURE

The instability is controlled by the Péclet number, defined as $\mathrm{Pe}=V_{O_2}h/D$. At Pe greater than some critical value Pe_c, the uniformly fed front is smooth [Fig. 6(a)]. As Pe is slightly decreased, small bumps that exist along the interface begin to compete over the oxygen, and the front develops a structure which marks the onset of instability [Fig. 6(b)]. When the oxygen supply is further decreased, lateral diffusion currents become important and the structure becomes periodic [Fig. 6(c)]. As the supply is further decreased, the peaks of the periodic structure deplete the oxygen in their vicinity, and separate into fingers [Fig. 6(d)]. This transition occurs at different number Pe_{c1}. The narrow band $\mathrm{Pe}_{c1}\leqslant\mathrm{Pe}\leqslant\mathrm{Pe}_c$ is the onset regime. It is characterized by a connected front with a cellular structure. The focus of this paper is on the developed fingering state $\mathrm{Pe}<\mathrm{Pe}_{c1}$.

Figure 6(d) shows a typical fingering pattern in the developed regime. The pattern develops by recurrent tip splitting. Combustion occurs only in the limited vicinity of the tips (in all the regimes) and there is no reaction behind the front (or along the fingers). Fingers that are closer to the oxygen source *screen* neighboring fingers. The screened fingers stop growing and the tips of the screening fingers split. The local dynamic mechanism for tip splitting is as yet unknown. We expect that the widening of the finger prior to the tip splitting will give some insight into this problem. The splitting maintains constant both the average finger width w and the spacing between fingers d.

As Pe is decreased, d grows. At a certain stage, d is sufficiently large to allow fingering without screening and we

obtain sparse fingers without tip splitting [Fig. 6(e)]. While w depends very weakly on Pe (for given h, it depends on h through the heat transport mechanisms), d is a rapidly decreasing function of it. The maximal value of d is comparable to the system size, $d \sim L$. The minimal value of d (zero) occurs at $\mathrm{Pe}=\mathrm{Pe}_{c1}$. Tip splitting is observed at $w \gtrsim d$.

A. Mass conservation

Since oxygen is the limiting factor, we expect all the available oxygen to be consumed by the front. We compare the mass of reacting gas per unit time Γ_{O_2} to the mass of reacting solid per unit time Γ_{solid}. If all the oxygen is consumed, then we have $\Gamma_{\mathrm{O}_2}=\mu\Gamma_{\mathrm{solid}}$. The proportionality factor μ is the stoichiometric coefficient, defined as the mass of reactant gas consumed by reacting with one unit mass of solid. Γ_{O_2} can be written in terms of the experimental parameters $\Gamma_{\mathrm{O}_2}=\int_0^L \rho_{\mathrm{O}_2} V_{\mathrm{gas}} a(h-\delta_{ub})dx$, where $\rho_{\mathrm{O}_2}(x)$ and $V_{\mathrm{gas}}(x)$ are the gas density and velocity, respectively, and a is the fraction of oxygen in the gas mixture. The integration is over the width of the sample L. Γ_{solid} is a function of the measured quantities $\Gamma_{\mathrm{solid}}=\int_0^L u(\rho_{ub}\delta_{ub}-\rho_b\delta_b)dx$, where $\delta(x)$ and $\rho(x)$ are the fuel thickness and density, respectively. The subscripts b and ub stand for burnt and unburnt solid, respectively. We thus expect that

$$\int_0^L \rho_{\mathrm{O}_2} V_{\mathrm{gas}} a(h-\delta_{ub})dx=\mu\int_0^L u(\rho_{ub}\delta_{ub}-\rho_b\delta_b)dx. \tag{3.1}$$

In the ''fingering'' regime the integral (per finger) is over $w+d$ in the left-hand side (LHS) and over w in the right-hand side (RHS) and we can approximate

$$\rho_{\mathrm{O}_2} V_{\mathrm{gas}} a(h-\delta_{ub})=\mu\frac{w}{w+d}(\rho_{ub}\delta_{ub}-\rho_b\delta_b)u. \tag{3.2}$$

A similar approach to Eq. (3.2) is used in the combustion of porous media [23]. With respect to the experimental driving parameter V_{O_2}, Eq. (3.2) can be written as

$$u\frac{w}{w+d}=AV_{\mathrm{O}_2}, \tag{3.3}$$

where the constant A (discussed in Sec. IV B below) represents the stoichiometry.

B. Lateral diffusion

In the perpendicular direction we expect diffusion currents, driven by the concentration gradients (see Fig. 7), given by $j_x=D\nabla_x C_{\mathrm{O}_2}$, where C_{O_2} is the oxygen concentration. The gradient is typically over a distance of $d+w$. At steady state, the lateral current satisfies $j_x=uC_{\mathrm{O}_2}$ up to a proportionality constant of order unity. This yields an equation for the velocity of the diffusion limited growth [12]

$$u=\frac{D}{(w+d)}. \tag{3.4}$$

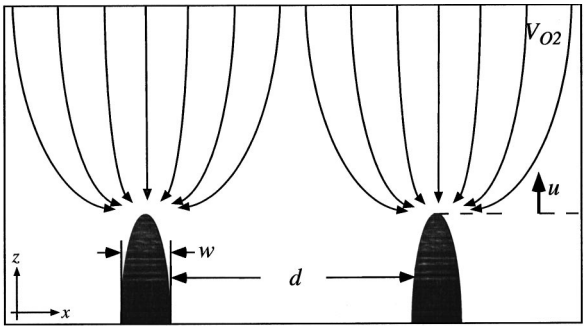

FIG. 7. The schematic flow field. The flow lines are diverted by lateral diffusion which is driven by the deficiency of oxygen at the tips.

The two growth conditions yield the following two nondimensional equations for the three quantities d, w, and u:

$$\tilde{d}=\sqrt{\frac{\tilde{w}}{A}}\mathrm{Pe}^{-1/2}-\tilde{w}, \tag{3.5}$$

$$\tilde{u}=\sqrt{\frac{A}{\tilde{w}}}\mathrm{Pe}^{-1/2}, \tag{3.6}$$

where $\tilde{w}=w/h$, $\tilde{d}=d/h$, and $\tilde{u}=u/V_{\mathrm{O}_2}$.

Equations (3.5) and (3.6) describe the growth with respect to the two horizontal directions. Experimentally the vertical direction (namely h) dictates w in a linear manner,

$$\tilde{w}\sim 1. \tag{3.7}$$

This enables a self-consistent evaluation of Eqs. (3.5) and (3.6). Equations (3.6) and (3.5) were experimentally verified to very good accuracy, assuming $\tilde{w}=1$ and without any fitting parameters [2].

C. Vertical convection

While there is no theory as yet for the role of heat transport away from the front, a number of observations point to its crucial role. We shall show later that the heat transport determines the width of the finger w. Equally important, we find that the occurrence of the fingering instability coincides with the arrest of free convection of gas in the gap. The flame tip is a heat source with a temperature of approximately $T_f=720$ K.

Convection at the tip, while extremely inhomogeneous, is determined by the Rayleigh number $\mathrm{Ra}=g\beta(T_f-T_{\mathrm{top}})h^3/\nu\alpha$. $T_{\mathrm{top}}\approx 450$ K is calculated by comparing the heat that is produced by the burning to the heat losses, latent heat of evaporation, and the heat needed to bring the paper to its evaporation temperature [2]. $\nu=0.5$ cm^2/s and $\alpha=0.5$ cm^2/s are the kinematic viscosity and thermal diffusivity, respectively, at the estimated gas temperature $T_{\mathrm{gas}}\approx 585$ K (estimated as the average of the top and flame temperatures). For an ideal gas, the volumetric expansion coefficient is $\beta\approx 1/T_{\mathrm{gas}}$. The onset of natural convection is expected at $\mathrm{Ra}_c\approx 1700$ (neglecting the applied wind and nonuniform heating). Experimentally, fingering occurs for $h\leqslant 1$ cm, i.e., $\mathrm{Ra}\geqslant 1810$. The rough numerical agreement is

an indication that fingering appears in the *absence of natural convection*. It also explains why the same phenomenon has been observed in a microgravity experiment in space [24].

IV. OXYGEN DEPLETION AND MASS CONSERVATION

In Ref. [2] we quantitatively verified Eq. (3.3) by comparing the influx of oxygen with the amount of reacted material. In the first subsection, we supplement this result with direct measurement of the percentage of oxygen in the gas behind the front. In the second subsection we detail the measurements of Ref. [2] and discuss other features of this measurement.

For additional results that concern oxygen depletion, see Sec. VII B on the ''coflow'' regime and Sec. VI B on the role of the nonreacting gas.

A. Direct measurement of oxygen content

In Fig. 8 we show a typical curve of the percentage of oxygen in the gas behind the front. Initially we placed the probe at the side of the sample to avoid interference with the growth [arrow in Fig. 8(a)]. As soon as the front passed the probe, we moved the probe to a position behind the front, so that the inlet is fed by the combustion products [arrow in Fig. 8(b)]. The results are shown in Fig. 8(c). Figure 8(d) shows the calibration curve for the probe. It shows the response time of the device (see caption for details). The experimental error is $\pm 10\%$ mainly because of the slow (5 s) response time of the detector. The same results are obtained when the measurement is done behind a finger (and not in the spacing between fingers). This measurement explicitly shows that all the oxygen is depleted by the front (within our 10% error). This result verifies the ''mass conservation'' Eq. (3.3).

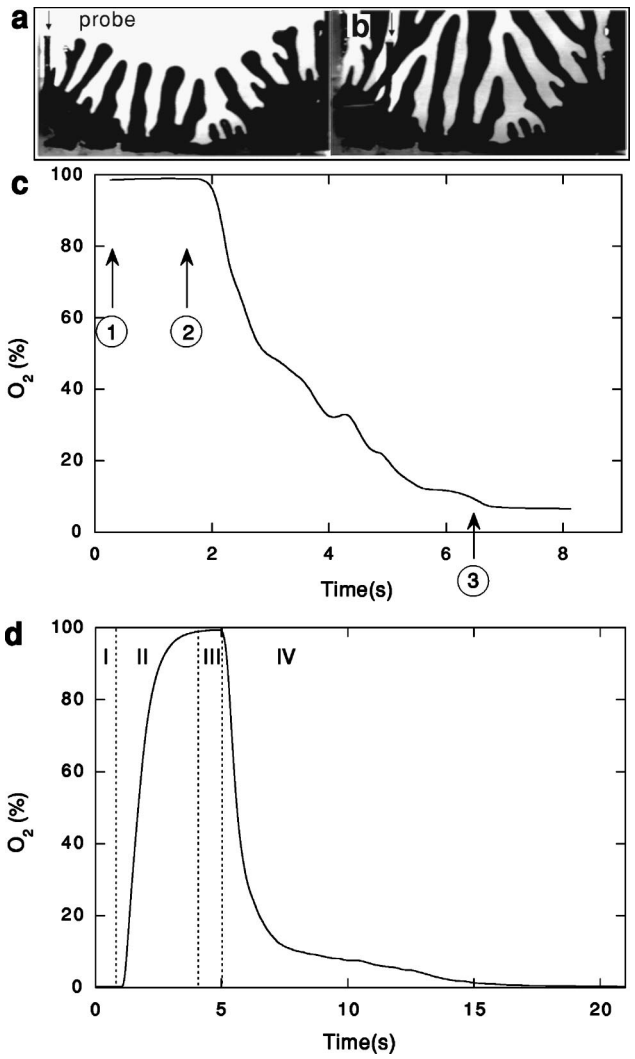

FIG. 8. Direct measurement of the relative oxygen content (using an electrochemical sensor) shows the depletion of oxygen (within 10% resolution). The probe's inlet is shown by the arrows in (a) (upstream the front) and (b) (downstream the front). (c) shows the relative oxygen content (in %): (1) ignition, (2) the front passes the probe, and (3) the front approaches the end of the sample. Between (1) and (2), the probe is near the boundaries, to avoid interference with the growth. At (2) the probe is moved to its position behind the front. This measurement was performed with the probe placed between the fingers. The same results are obtained when it is placed on the fingers. *d* shows a calibration curve for the relative oxygen content in the gas (no flame): *I*, initial flow of 100% N_2 ($a=0$, $f_{N_2}=3$ cm/s). The response to an abrupt change to 100% O_2 ($a=1$, $f_{O_2}=3$ cm/s) is shown in *II* (increase) and *III* (stable part). *IV* shows the transition back to 100% N_2.

B. Comparing the fluxes

The verification of the ''mass conservation'' is based on measuring the LHS of Eq. (3.3) as a function of V_{O_2} [2]. The results are shown in Fig. 9. The corresponding front velocity u is shown in the inset. Below a critical value corresponding to Pe_{c1} (arrow in the figure), u is proportional to $(V_{O2})^{1/2}$ as predicted by Eq. (3.6). At Pe_{c1} there is a crossover to the linear dependence predicted by Eq. (3.3) with $d=0$. Equation (3.3) predicts a linear dependence of the quantity of burnt material per unit time $uw/(w+d)$ on V_{O_2} with the slope being the stoichiometric factor A, given by

$$A=\frac{a\rho_{O_2}(h-\delta_{ub})}{\mu(\rho_{ub}\delta_{ub}-\rho_b\delta_b)}. \tag{4.1}$$

In the following we detail the evaluation of the stoichiometric factor A. The values that we used are $a=1$ (99.99% oxygen), $\rho_{O_2}=1.376\times10^{-3}$ g/cm^3 [30]; paper thickness and density are $\delta_{ub}=0.018\pm0.001$ cm and $\rho_{ub}=0.66\pm0.05$ g/cm^3 (direct measurement over 10 samples, the manufacturer's data are $\delta_{ub}=0.019$ cm, $\rho_{ub}=0.54$ g/cm^3). The thickness and density of burnt paper are $\delta_b=0.01\pm0.003$ cm and $\rho_b=0.3\pm0.03$ g/cm^3. These values of δ_b and ρ_b represent averages over 10 runs.

It is interesting to point out that δ_b and ρ_b are not constant. Both depend weakly on V_{O_2}. Both quantities increase in the V_{O_2} range of $0.5-15$ cm/s but do not change by more than 20% over that V_{O_2} range (this adds some error to our measurement of A). At higher flow rates the burning is more efficient and both quantities significantly decrease. Near extinction the burning is slow but more material is converted. Therefore δ_b and ρ_b decrease. The minimum is obtained for $V_{O_2}=0.06$ cm/s, where full conversion is reached, i.e., $\delta_b=0$ and $\rho_b=0$.

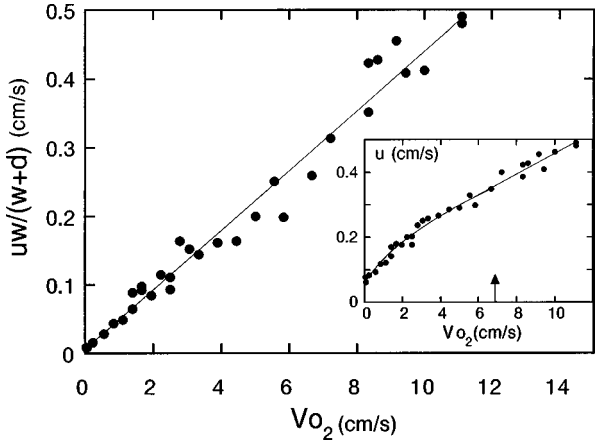

FIG. 9. Mass conservation, as predicted by Eq. (3.3) (solid line). The inset shows u as a function of V_{O_2}. The arrow corresponds to Pe_{c1} (onset of separated fingers). The molecular diffusion coefficient of oxygen is $D=0.25$ cm^2/s (neglecting its temperature dependence).

We calculate a stoichiometric coefficient $\mu=1.18$ for the interaction of oxygen and cellulose (which comprises 98% of the paper). We used $(C_6H_{10}O_5)n+6nO_2\rightarrow(6CO_2+5H_2O)n$. The above calculation is based on the assumption that the chemical composition of the parts of the paper that is left unburnt does not change significantly. To check this assumption we analyzed the CH composition of the charred and unburnt paper [29]. For unburnt paper we found 44.78% (C), 6.22% (H), and 49.4% (O+others) (as expected from $98\%\times C_6H_{10}O_5$). For burnt paper we found 42.56% (C), 6.38% (H), and 51.1% (O+others), i.e., the assumption is justified.

Combining the above numbers we obtain $A=0.051\pm0.005$. Given the complications of this calculation and measurement, the numerical agreement (within experimental error) with the measured slope $A=0.043\pm0.005$ in Ref. [2] is satisfactory. It shows that the system is well within the oxygen deficient regime.

V. THE SPACING BETWEEN FINGERS: COMBINING DRIFT WITH LATERAL DIFFUSION

A. The effect of Pe

In Sec. III (Fig. 6) we have shown the behavior of the pattern as a function of Pe at $(0\leqslant\mathrm{Pe}\leqslant\mathrm{Pe}_c)$. In this subsection we focus on the fingering regime $0\leqslant\mathrm{Pe}\leqslant\mathrm{Pe}_{c1}$ [(d) and (e) in the figure]. The variation of d as a function of Pe in this regime is exemplified in Fig. 10. (a) shows the minimum value ($d=0$) at the onset ($\mathrm{Pe}\sim\mathrm{Pe}_{c1}$). (b) shows the minimal detectable nonzero value of d. The tip splitting regime starts at $\mathrm{Pe}<\mathrm{Pe}_{c1}$ [(c)–(f) in Fig. 10]. In (g) the distance between fingers is large enough to allow fingering without tip splitting. The value of d increases as we decrease Pe until its maximal value, which is comparable to the size of the system L [Fig. 10(i)].

The above results are quantified in Fig. 11. The figure shows the dependence of d and w on Pe. The continuous line shows the theoretical prediction [Eq. (3.5)]. It is in very good agreement with the data points. These measurements were performed by varying V_{O_2} at $h=0.5$ cm. Other values of h (in the range 0.2 cm$\leqslant h\leqslant$1 cm) show the same qualitative dependence of d on Pe. The finger width shows a very slow (linear) increase with Pe (at fixed h).

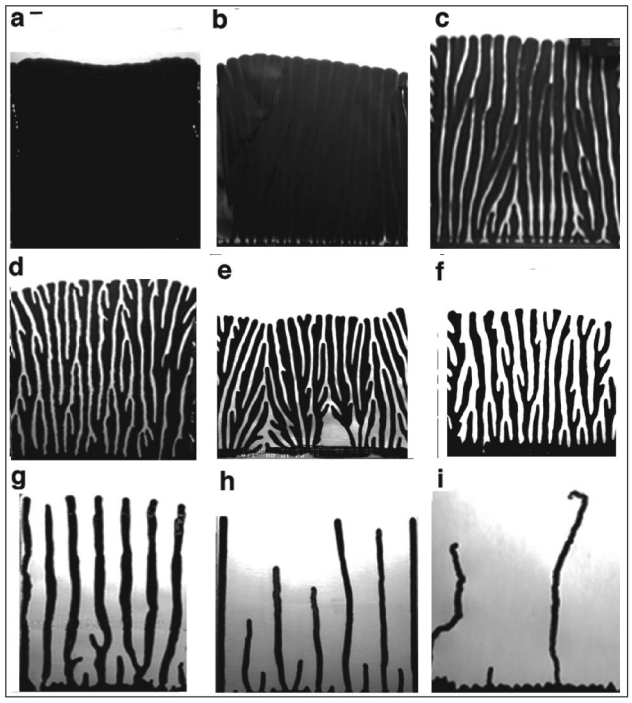

FIG. 10. Collage of patterns showing the full variation of d ($0<d\leqslant L$) as a function of Pe [decreasing from (a) to (i)]: (a) near the onset ($\mathrm{Pe}\approx\mathrm{Pe}_c$) $d=0$, (b) slightly below the onset ($\mathrm{Pe}\lesssim\mathrm{Pe}_{c1}$) $d\rightarrow0$, (c)–(f) fingering with tip-splitting, (g)–(i) fingering without tip-splitting. The values of Pe [(a)–(i)] are 18, 15, 14, 11, 9 ± 1, 5 ± 0.5, 1.5 ± 0.25, 0.45 ± 0.2, 0.07 ± 0.02. The spacing between plates is $h=0.5$ cm in all the figures except (c) and (e), where $h=0.6$ cm.

Figures 10 and 6 show that the value of Pe determines the ratio between w and d, which characterizes the pattern.

(i) Sparse fingers (fingering without tip splitting) are observed at $d/w\gg1$, which corresponds to $0.1\lesssim\mathrm{Pe}\lesssim2.6$.

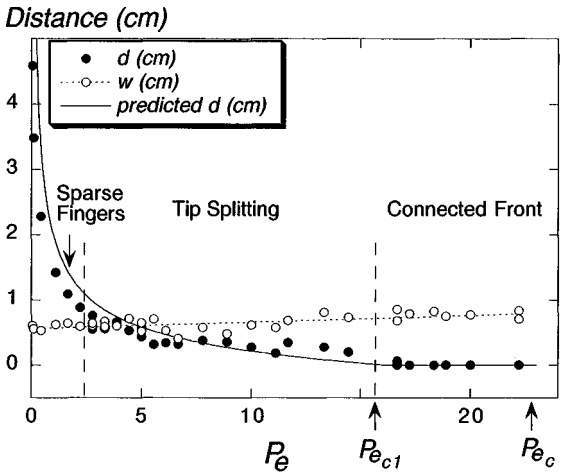

FIG. 11. The distance between fingers d (full circles) and finger width w (empty circles) as a function of Pe. d is determined by the driving parameter, while w is only weakly influenced by it. The continuous line is a plot of the RHS of Eq. (3.5) with $A=0.043$ (see Fig. 9) and the dashed line is $w=0.56+0.01\mathrm{Pe}$ (in cm).

(ii) Tip splitting is observed at $\frac{1}{4} \leqslant d/w \lesssim \frac{5}{4}$, which corresponds to $2.6 < \mathrm{Pe} \lesssim \mathrm{Pe}_{c1}$.

(iii) The onset of fingering (breakage of a ''connected front'') is observed for $\mathrm{Pe} < \mathrm{Pe}_{c1}$. Experimentally $\mathrm{Pe}_{c1} = 17 \pm 1$. The predicted value [obtained from Eq. (3.5)] is $\mathrm{Pe}_{c1} = 1/Aw \approx 21$ [2].

(iv) A connected front is observed at $\mathrm{Pe}_{c1} \leqslant \mathrm{Pe} \leqslant \mathrm{Pe}_c$. In this regime $d = 0$ and w is the characteristic ''cusp'' size. Experimentally $\mathrm{Pe}_c = 22 \pm 1$ [31].

(v) w and d are not defined for $\mathrm{Pe} \geqslant \mathrm{Pe}_c$.

B. A fundamental relation with another diffusion-limited system: Electrochemical deposition

The dependence of d on Pe was obtained from Eqs. (3.3) and (3.4), which describe quite generally the growth under a limited supply of reactants. It is reasonable to expect this simple consideration to apply to other systems with similar conditions. In this section we describe preliminary results (analyzing previous experiments of ours [26,27]), which show that the distance between branches in electrodeposition behaves as the distance between fingers in combustion.

Electrodeposition is a well known example of diffusion-limited growth [26,27,32,33]. The experiments are usually conducted in a quasi-two-dimensional cell, filled with an ionic solution (usually zinc or copper) of concentration C. The growth is controlled by the electric current density j.

Our experiments show decoupling between the structure of a single branch (microstructure) and the macroscopic structure. The microstructure can be dendritic or disordered (tip splitting), depending mainly on the concentration. The macroscopic structure consists of sparse or dense fingers, depending mainly on j. At low currents the fingers are sparse (large d), while at high currents the fingers are dense (small d). Figure 12 shows three pictures that illustrate this result (near the dense regime in electrodeposition of zinc).

It is straightforward to apply the phenomenological model of Eqs. (3.3) and (3.4) to electrodeposition. The mass conservation equation reads

$$uw = V(w+d), \tag{5.1}$$

where V is the velocity of the ions and z the ion charge. The lateral diffusion equation is exactly as in Eq. (3.4). We obtain the same square root dependence:

$$d = \sqrt{\frac{wh}{\mathrm{Pe}}} - w. \tag{5.2}$$

The calculation of Pe is based on the relations $J = \sigma E$ and $V = \mu E$, where σ is the electric conductivity, E is the electric field, and μ is the ion mobility. We obtain

$$\mathrm{Pe} = Vh/D = \frac{\mu}{\sigma}\frac{h}{D}J. \tag{5.3}$$

To find μ/σ we measured $u(w/w+d)$ as a function of J and obtained $\mu/\sigma = 0.018 \pm 0.005$ cm^3/Coulomb. The diffusion constant was taken to be $D = 1.3 \times 10^{-5}$ [30].

In Fig. 13 we show a measurement of d and w as a function of Pe. The continuous line is the prediction of Eq. (13), which we wrote as $d = \alpha\sqrt{wh/\mathrm{Pe}} - w$ with α as a fitting parameter. In Fig. 13, $\alpha = 3.5$. In the combustion experiment the agreement was good without any fitting parameters, while here the results are only indicatory due to the small statistical sample. These results show that the complex small scale processes are decoupled from the large scale diffusive transport that determines the distance between fingers.

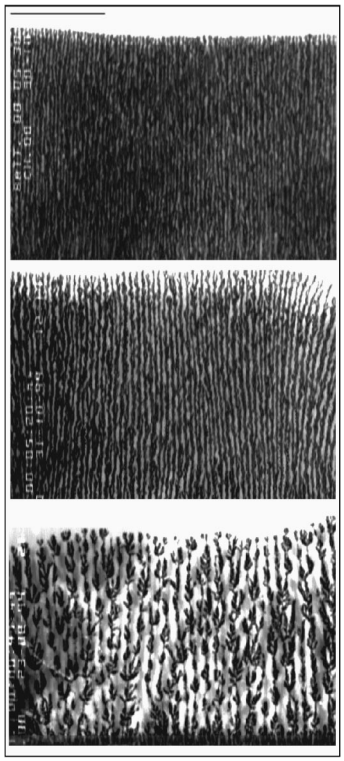

FIG. 12. Diffusion limited growth in electrodeposition. The figure shows the influence of current density J, at a fixed ionic concentration ($C = 0.03$ M) on the density of fingers. The current densities (bottom to top) are $J = 13.3$, 116, and 197 mA/cm^2. The figure shows the decrease of spacing between fingers d as a function of J.

This result can be generalized to include other systems that are diffusion limited and supplied by constant flux.

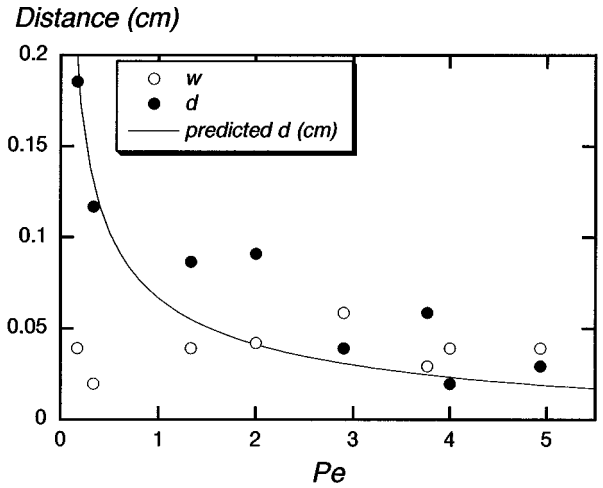

FIG. 13. The behavior of d and w as a function of Pe in electrodeposition is similar to what we obtained in combustion. Notice that the front is not connected ($d > 0$) even at high current densities J (and Pe). We conjecture that this result is related to the depletion of ions. The fitting parameter for the continuous line is $\alpha = 3.5$.

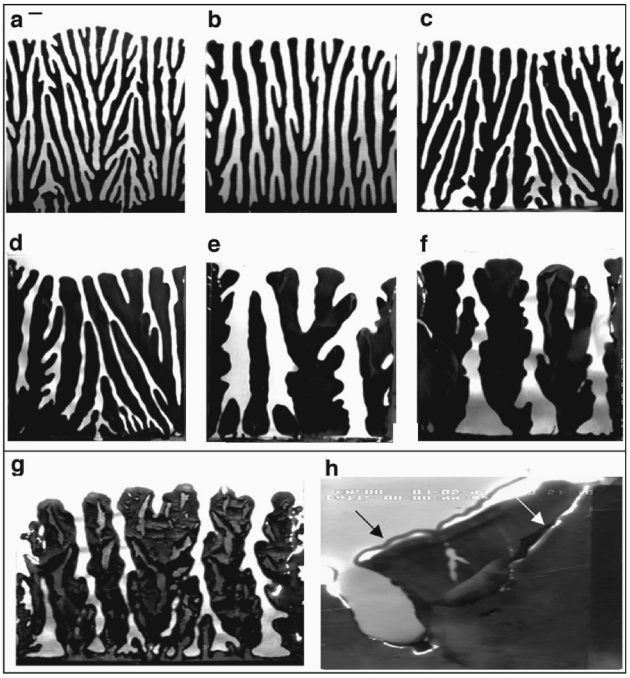

FIG. 14. The variation of the finger width w as a function of the spacing between plates. $h=0.2$, 0.3, 0.5, 0.6, 0.8, and 1 cm in (a) to (f), respectively. In (g) we show the thickest fingers that we obtained ($h=1.8$ cm). At this value of h the burning is not uniform. In (h) we show some of the 3D effects that occur at higher values of h (here $h=3$ cm). There is more than one front (arrows in the figure), the burning is not uniform, and there are no fingers.

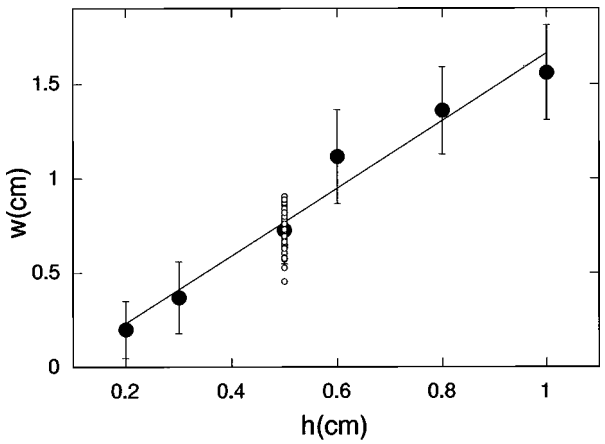

FIG. 15. Finger width w as a function of h. The different points were measured in various V_{O_2} and flux ($h\times V_{O_2}$) values. As already shown in Fig. 11, V_{O_2} does not change w by more than 15%. To accentuate this, we show the data points of Fig. 11 (empty circles at $h=0.5$ cm). They show the result of varying V_{O_2} alone. The slope of $w(h)$ is 1.78 ± 0.2. The error bars represent the spread of the experimental results.

VI. THE FINGER WIDTH: HEAT LOSSES

We have shown that d is determined by the flux of reactants (through Pe) and that w is almost independent of Pe. w is a feature of the individual finger that is determined by the ability of the front to release heat. We now show that w is related to the heat losses in the system.

A. The role of two dimensionality

The instability occurs below a critical Ra and therefore below a critical h. The weak dependence of w on Pe allows us to measure w as a function of h over a wide range of Pe. In Fig. 14 we show a collage of the fingering patterns that results from varying h. The pictures were taken in the Pe range of $7\lesssim \mathrm{Pe}\lesssim 12$, which is well within the tip-splitting regime. h is increased from a minimal value of 0.2 cm [Fig. 14(a)] to the maximal value at 1 cm [Fig. 14(f)]. Going below $h=0.2$ cm raises several experimental complications. It reduces the uniformity of the flow as well as the uniformity of the exchange of heat with the top plate. The upper limit of h is determined by Ra. In Fig. 14(g) we show the thickest fingers that we obtained ($h=1.8$ cm), which were still well defined but the burning is not uniform throughout the paper and the reproducibility of the measurement is reduced. At higher values the fingering instability no longer exists, as shown in Fig. 14(h). In this picture $h=3$ cm. There is more than one front (arrows in the figure), the burning is not uniform, and there are no fingers. These effects are due to the vertical flow of oxygen that feeds the burning behind the front.

To quantify the relation, described above, between w and h, we first notice that Fig. 11 shows that as $\mathrm{Pe}\to 0$, w approaches h, i.e., $\tilde{w}=\alpha+\beta\,\mathrm{Pe}$ with $\alpha\approx 1$ and $\beta\ll 1$. The smallness of β allows us to conduct the measurement of w as a function of h in the full range of Pe. Figure 15 shows the results. The data are consistent with linear dependence. The measured slope of $w(h)$ is 1.8 ± 0.4. The linear dependence of the characteristic length of the instability on the spacing between plates is also known from other growth systems in quasi-2D (''Hele-Shaw'') geometry [3,11].

B. Other heat losses

In this subsection we study the influence of two other heat release mechanisms that can be experimentally controlled: (i) Changing the heat conductivity of the bottom plate; (ii) adding nonreacting gas to the front. Our goal is to see whether these experimental measures support our picture.

To study the influence of the bottom plate, we used bottom plates made of Cu, Al compound, and Pyrex glass ($\lambda=4\times10^7$, 2.4×10^7, and 6.3×10^5 erg/cm s K, respectively). The heat conductivity of the ambient gas is two orders of magnitude smaller ($\lambda\approx 2.6\times10^3$ erg/cm s K). We concluded that there is no significant variation of w in this range of λ. Using no bottom plate caused a notable increase in w but involves the presence of reactant gas below the sample. This has an influence on the flow pattern near the front. To create a heat isolating bottom without these effects, we used a thin (0.004 cm) stainless steel foil. The contribution to heat release was small and the 3D effects were prevented. In this measurement we saw an increase in w.

These effects are shown in Figs. 16(a)–16(c). (a) shows a typical pattern using an aluminum bottom plate ($\mathrm{Pe}=5$, $h=0.5$ cm). (b) shows a run with the same parameters using a thin foil instead of a bottom plate as described above. In (c) there is no bottom plate and the sample is stretched above a recess containing the ambient gas. The figure shows an increase in w from (a) to (b), which qualitatively shows that

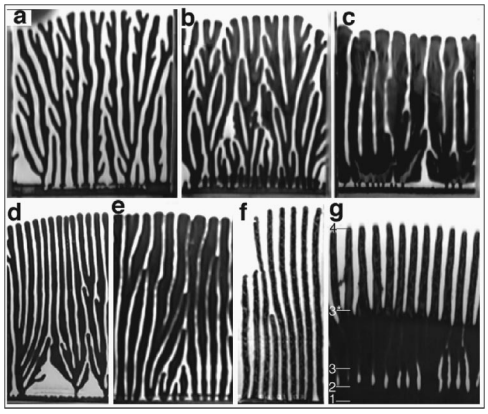

FIG. 16. The effects of heat losses on the pattern are measured both by changing the bottom plate [(a)–(c)] and by changing the N_2 content of the reacting gas (d)–(f). (a) Typical pattern using aluminum bottom plate (Pe$=5\pm0.5$, $h=0.5$). (b) Same parameters as in (a) with the bottom being a thin foil. w increases from (a) to (b). (c) No bottom plate, only air in the cavity. This involves 3D effects which have to be taken into account when comparing (c) with (a) and (b). (d), (e) Two runs with and without nitrogen $f_{O_2}=7$ in (d) $a=0.86$ and in (e) $a=1$. Adding N_2 decreases w. In (f) we see that in a run with $f_{O_2}=5$, $a=0.76$ tip splitting is suppressed. (g) shows the effect of variation during a run: $1-2$ ignition ($f_{O_2}=15$ cm/s, $a=1$), $2-3$ only oxygen ($f_{O_2}=6$ cm/s, $a=1$), $3-4$ oxygen +nitrogen ($f_{O_2}=6$ cm/s, $a=\frac{5}{8}$). In the final state the effect of nitrogen is a 20–30 % decrease in w. In $3-3^*$ we show the transition from $a=1$ to $a<1$. The fingers become effectively wider and w increases temporarily until, without changing the external supply, it decreases to a new value of w that corresponds to $a<1$ [for more observations that concern this effect, see Fig. 22(g) in Sec. VII]. We conjecture that the transient effect is related to the effectively improved transport of O_2 which result from switching on the N_2 flow.

the ability to release heat narrows w. The result shown in (c) involves the 3D effects of gas flow, which should be taken into account when comparing (c) with (a) and (b).

A more controlled way to study the effect of heat losses is by adding cooling (nonreacting) gas to the flow. We found that adding nitrogen to the flow (at fixed f_{O_2}) has two main effects: (i) w decreases, and (ii) tip splitting is suppressed. These effects are shown in Figs. 16(d)–16(g). In (d) and (e) we see two runs with the same values of Pe (14 ± 1, defined for the combination of oxygen and nitrogen Pe $=V_{(O_2+N_2)h}/D$). In (d) we added 20% nitrogen ($a=0.83$), while in (e) $a=1$. The figure shows that the result of adding N_2 is a decrease in w. To some extent it also shows the suppression of tip splitting. Figure 16(f) shows a run with Pe$=5.8$ and $a=0.76$. We have already shown that this value of Pe (and d/w) is well within the tip-splitting regime for $a=1$. The figure shows that an effect of $a\neq1$ is the suppression of tip splitting.

The abrupt addition of nonreacting gas has an interesting transient effect. This is shown in Fig. 16(g). The values of V_{O_2} and a were varied within the run in the following manner: $1\rightarrow2$ ignition ($V_{O_2}=15$ cm/s, $a=1$), $2\rightarrow3$ only oxygen ($V_{O_2}=6$ cm/s, $a=1$), $3\rightarrow4$ oxygen+nitrogen ($V_{O_2}=8$ cm/s, $a=6/8$).

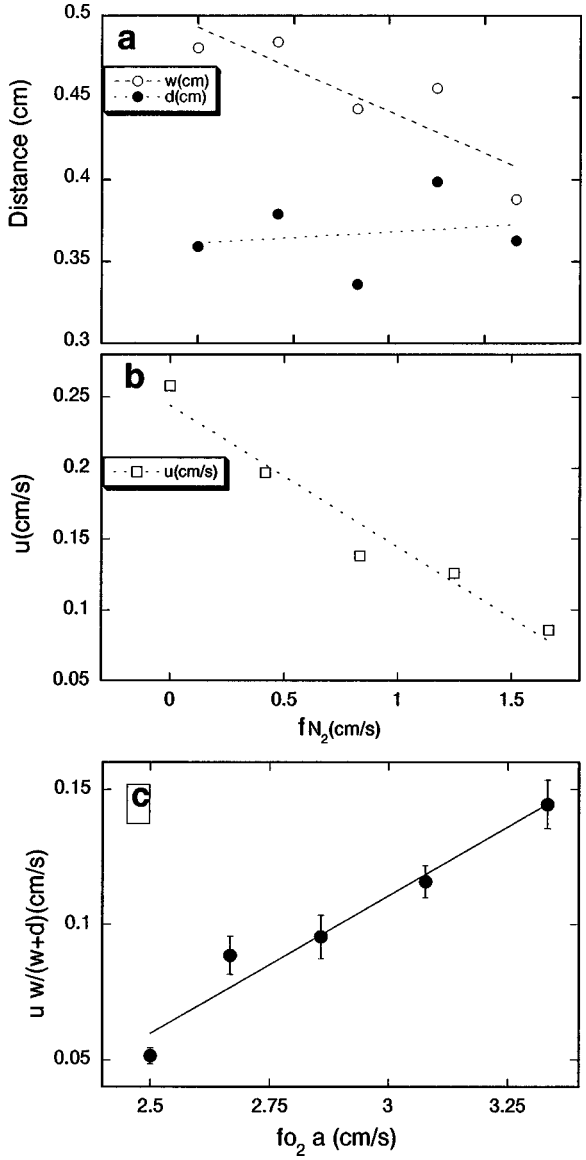

FIG. 17. The effect of cooling, nonreactant gas is shown at fixed $f_{O_2}=5$ cm/s. (a) w is a decreasing function of f_{N_2} while d is not affected by it (within experimental error), (b) u is a linearly decreasing function f_{N_2}, (c) the burning ''intensity'' is linear in $a\times f_{O_2}$ as expected from ''mass conservation.'' The slope is $A=0.08\pm0.01$ (prediction $A=0.051\pm0.004$).

In $3\rightarrow3^*$ we show a transient state as the system goes from $a=1$ to $a<1$. The fingers become wider (almost merging) until they spontaneously (i.e., without any change in the external supply) decrease to the new value of w that corresponds to $a<1$ [for more observations that concern this effect, see Fig. 21(g) in Sec. VII]. We conjecture that this effect is related to the initially improved transport of O_2, which results from enhancing the flow. In the final state ($3^*\rightarrow4$) the effect of nitrogen is a 20–30 % decrease in w.

Figure 17 quantifies the effect of adding nonreacting gas. In (a) we see the effect on d and on w. In (b) we see the effect on u and in (c) on the rate of burning. Within error bars, we see that w decreases as a function of a, while d does not change significantly. These results are consistent with our picture that w is a decreasing function of the ability of the front to release heat.

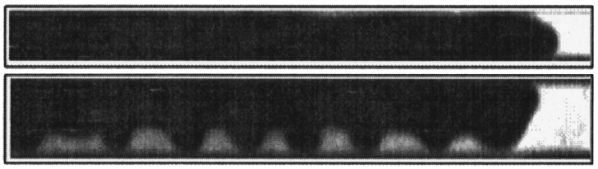

FIG. 18. The instability of an isolated finger ($w=0.5$ cm) is manifested as a periodic attempt to tip split in a thin paper of width $L=1$ cm (bottom). It does not occur at $L=0.6$ cm (top). The distance between the two stripes was 10 cm, ensuring no interaction between them ($h=0.5$ cm, Pe = 6).

The linear decrease of u and of the amount of burnt material can be compared to the mass conservation equation [Eq. (3.3)]. We write this equation as

$$\tilde{u}\frac{w}{w+d}=Aa. \tag{6.1}$$

Figure 17(c) shows a plot of $u(w/w+d)$ as a function of $f_{O_2}a$ at fixed $f_{O_2}=3$ cm/s. The linear behavior is as predicted. The slope is $A=0.08\pm0.01$ (prediction from stoichiometric considerations: $A=0.051\pm0.004$). The discrepancy may be due to other effects of the addition of N_2 that we may be missing.

We point out that the highest percentage of N_2 that allowed flame propagation in our system was 40% (at $h=0.6$ cm). This result is expected to be relevant for studying the occurrence of the fingering effect under atmospheric conditions.

There is at present no theoretical framework that accounts for the experimentally observed connection between the heat losses and finger width. A first step is to derive w by comparing the heat losses from an isolated finger to the heat that is released by the combustion of that finger. The main heat loss channels that should be taken into account are (i) advection of hot gases by the wind, (ii) conduction from the hot surface to the wind, (iii) conduction through the bottom plate, (iv) conduction through the sample, (v) radiation from the front. The dominant channels are obviously (i) and (iii). So far the comparison between the produced and dissipated heat has shown only qualitative agreement. Precise measurements of local heat production and loss will be necessary to obtain a quantitative description.

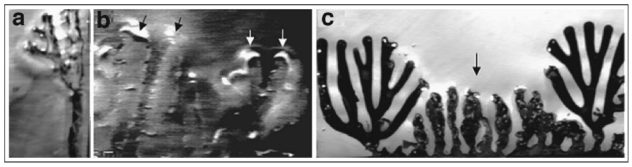

FIG. 19. Fingering in other fuels. (a) Made of cellulose acetate, (b) polyethylene. In polyethylene there is a strong effect of melting and a glowing, nonuniform combustion. The arrows mark the fingers. The contrast was enhanced because of the low quality of the image. (c) Stationery paper 80 gr/m^2 (chlorine bleached). The arrow points at a region that wrinkles and produces a different pattern with a different, nonuniform reaction (not smoldering).

C. An isolated finger

To check the coupling between d, which is determined by the collective competition over oxygen, and w, we forced the system to produce isolated fingers (Fig. 18). We placed strips of paper whose width was on the order of the height of the cell, and placed them far enough so that they did not interact (about three fingers per run). The figure shows that w is selected at the level of a single finger. Fronts with different paper width propagated at the same velocity u and with the same w as the main trunk in the wide system (within experimental scatter). At $L=1$ cm (bottom) we observe periodic attempts to tip split, which cannot be accomplished (since $L<w+d$). We conclude that the instability is not a collective effect but a local feature involving a single finger, and that the competition over oxygen determines d but not w.

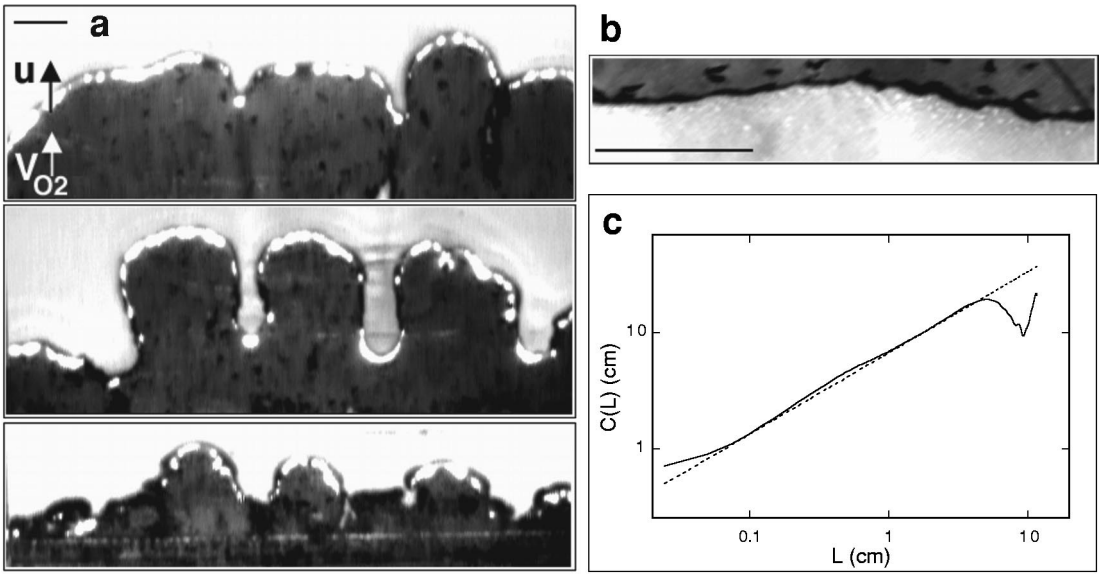

FIG. 20. (a) Evolution in the *coflow* regime. Times from ignition (bottom to top): 60 s, 72 s, 118 s. $V_{O_2}=10.2$ cm/s, $u=0.31$ cm/s. The fingers are transient. The steady-state front is linearly stable (top figure). (b) In the stable front we extinguished the fire and obtained a snapshot of the noisy front. (c) The correlation function for the interfaces as shown in (b) computed for five runs. The scale bars are 1 cm.

VII. OTHER OBSERVATIONS

In this section we present a number of observations that highlight some of the unique features of this system, as well as providing additional information on the issues that we discussed above.

A. The effect of changing fuel

It is essential for practical implications to know the effect of different fuels. We have checked various materials ranging from stationery paper to plastics. All the materials that we checked exhibited the fingering effect. Figure 19 shows fingering patterns in a dialysis bag (a), in a polyethylene sheet (b), and in stationery ($80\ \mathrm{g/m^2}$) paper (c).

Our measurements were mostly performed with paper produced by Whatman. We mostly used grade no. 2 (thickness $\delta=0.019$ cm, ash%$=0.06$). We also studied grades no. 1, 2, 3, 40, and 91. Grade no. 3 is similar to no. 2 but with $\delta=0.039$ cm. The change of paper thickness had only a minor effect on our results of d, w, and u. Grade no. 40 is ''ashless'' (ash% $= 0.007$). This affects the color of the pattern, which tends to be more ''brown'' than ''black.'' Grade no. 91 is highly anisotropic. This reduces the uniformity and reproducibility but otherwise did not have any significant effect on the pattern.

B. The coflow regime

Our setup allows us to perform measurements when the front propagates with the wind (coflow regime). In this regime the front is slower and more stable. This counterintuitive result is related to the fact that the combustion is more intense and all the fuel is consumed (no char is left). Figure 20 shows the typical evolution in the coflow regime. The front is initially unstable. However, the fingers that develop are a transient state. After the transient the fingers merge.

Stable or marginally stable fronts sometimes exhibit a roughness exponent that characterizes the growth mechanism [34,35]. In Fig. 20(b) we show a picture of the front in the developed state. The height-height correlation function $C(L)$ is shown in (c). It extends over two decades, showing that $C(L)\sim L^{\chi}$ with $\chi=0.66$ (average over five measurements). Correlations in coflow flames (parallel to gravitational connection) were measured previously in the context of the Kardar-Parisi-Zhang (KPZ) model [34,36].

We checked that mass conservation [Eq. (3.3)] holds also in the coflow regime (with $w/w+d=1$ and $\delta_b=0$). That is, $u=AV_{\mathrm{O}_2}$, where $A=\rho_{\mathrm{O}_2}(h-\delta_{ub})/(\mu\rho_{ub}\delta_{ub})$. With the above data, $A=0.039$. Our measurements in the coflow regime yield a slope of $A=0.045\pm0.05$, in rough agreement with the calculation.

C. Other features of the pattern

There are many qualitative observations that we have not described previously. These observations were performed in runs that had nonuniformities or ''defects'' and were not used for the quantitative analysis. Yet they contain significant information on various features of this effect. In Fig. 21 we show a collage of these observations. (a) and (b) show the effect of nonuniformity on the pattern. (a) shows the effect of nonuniformity in the initial conditions (arrow in the figure).

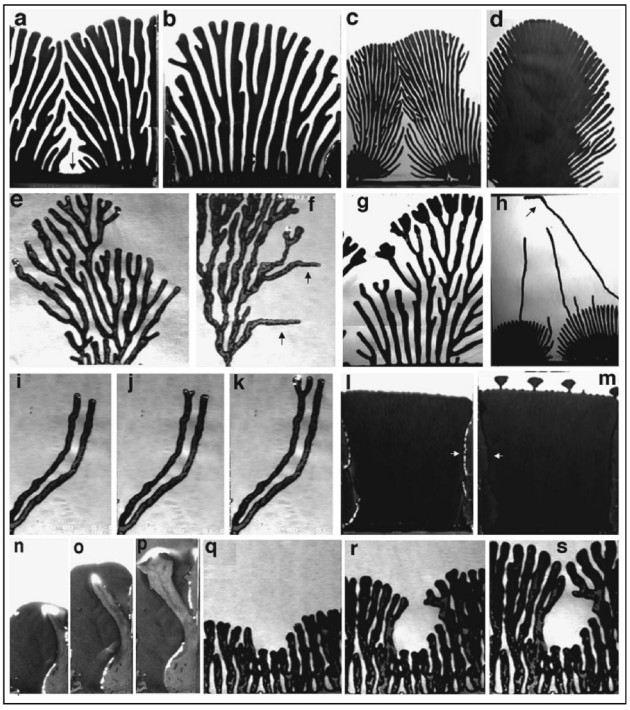

FIG. 21. Qualitative observations with nonuniformities. (a) A defect line with a concave front, (b) convex pattern from a nonuniform gas flow, (c) ''merging'' of clusters, (d) nonuniform ignition and flow near the onset, (e) ''cluster screening,'' (f) interaction with a horizontal grid, (g) response to a change from 100% O_2 to 100% N_2, (h) changing from Pe = 6 to Pe = 0.08, (i)–(k) two fingers tip split near extinction, (l) above onset with free boundaries, (m) the extinction of (l), (n)–(p) ''secondary'' finger with large h, (q)–(s) growing past an obstacle.

The result is a concave front with a ''defect'' line. (b) shows the convex pattern that results from a nonuniform gas flow. The experimental parameters for (a) and (b) were Pe = 8, $h=0.6$, and Whatman paper no. 3. (c) shows the growth of two clusters that were ignited at the two ends of the sample. (d) shows a pattern near the onset that was ignited in the middle and grew in a nonuniform flow field. The ''side branching'' is due to the nonuniformity. (e) shows how there is screening of ''clusters'' in a nonuniform field and not only of fingers. (f) shows a run in which we attached a horizontal grid of stick tape to the bottom plate. The pattern is seen to interact with the underlying grid. (g) shows a run in which we changed the supply abruptly from 100% O_2 to 100% N_2: w initially increases and d decreases, due to the improved transport of O_2 [see Fig. 16(g)]. Then the fingers narrow down until extinction. In (h) we show the transition that occurs by cutting Pe abruptly to 0.08 in the middle of a run, with nonuniform ignition. The single finger that prevails propagates horizontally at the edge of the sample. In (i), (j), and (k) we show two fingers that evolve from a single branch, after nonuniform ignition near extinction (Pe $=1$). They slowly grow together until a fluctuation causes the left finger to prevail, driving tip splitting. Notice the bright spots on the tips. In the tip-splitting regime these spots typically appear before the extinction of a finger [see also Fig. 6(e)]. In (l) we show propagation slightly above onset. In this run we did not use our ''normal'' boundary conditions (which are heat conductive and slightly elevated), but left the bound-

aries free. Consequently, we observe a glowing flame that propagates inwards from the lateral boundaries of the paper (arrows in the figure). (m) shows the same pattern after the oxygen was cut and nitrogen fed in (after about 5 s). The cutting of oxygen (from Pe = 18 to Pe = 0) causes a gradual decrease of w and selection of d. Then we fed 100% of N_2 ($a=0$) and w grew until extinction. (n), (o), and (p) show a 3D effect: propagation of a finger with a glowing flame in the char, in a system with a very large gap between the plates ($h=3$ cm). (q), (r), and (s) show how the pattern grows past an obstacle. The obstacle is a part in the paper that has a ''crumple'' that blocks the oxygen flow.

VIII. SUMMARY AND CONCLUSIONS

We detailed the previously reported fingering instability in combustion, which occurs when a solid fuel (e.g., paper) is forced to burn against an oxygen-rich wind, below a critical Ra. The nondimensional control parameter of the effect is the Péclet number.

The two length scales of the system are decoupled: The spacing between fingers is determined by the Péclet number. This dependence quantitatively verifies a phenomenological model which we base on reactant transport (without any fit parameters). The same model qualitatively applies to electrochemical deposition.

Within the phenomenological model that disregards heat losses, the finger width is independent of the Péclet number. It is linearly dependent on the system height. This quantitative dependence is in line with qualitative observations which show that the finger width is determined by the ability of the front to release heat.

For further experimental research we point out the behavior near the onset, where our preliminary observations have already shown interesting spatiotemporal modes. Another experimental challenge is to expand our analysis to other growth systems.

From the theoretical viewpoint, there is still a need for a linear theory of the instability. The analogy between electrodeposition and combustion opens the possibility for a universal description of some aspects in diffusion limited growth. This should go along with a theoretical identification of the class of instabilities that exhibit the behavior described in this paper.

ACKNOWLEGMENTS

We take pleasure in thanking J.-P. Eckmann, J. Fineberg, B. Greenberg, T. Kashiwagi, B. Matkowsky, G. Sivashinsky, and V. Steinberg for fruitful discussions. Special thanks are due to Z. Olami who collaborated on the phenomenological model in combustion.

[1] M. Faraday, *The Chemical History of a Candle*, edited by W. Crookes (Chatto & Windus, London, 1882).
[2] O. Zik, Z. Olami, and E. Moses, Phys. Rev. Lett. **81**, 3868 (1998); O. Zik, Ph.D. thesis, The Weizmann Institute of Science, 1998 (unpublished); O. Zik and E. Moses, *Proceedings of the 27th International Symposium on Combustion* (The Combustion Institute, Boulder, 1998), pp. 2815–2820.
[3] P. Pelce, *Dynamics of Curved Fronts* (Academic Press, Boston, 1988).
[4] J. Krug and H. Spohn, *Solids Far From Equilibrium* (Cambridge University Press, Cambridge, 1992).
[5] A.-L. Barabasi and H. E. Stanley, *Fractal Concepts in Surface Growth* (Cambridge University Press, Cambridge, England, 1995).
[6] T. Halpin-Healey and Y.-C. Zhang, Phys. Rep. **254**, 215 (1995).
[7] Y. Couder, in *Chaos, Order and Patterns*, edited by R. Artuso, P. Cvitanovic, and G. Casati (Plenum Press, New York, 1991), p. 203.
[8] W. W. Mullins and R. F. Sekerka, J. Appl. Phys. **35**, 444 (1964).
[9] J. S. Langer, Rev. Mod. Phys. **52**, 1 (1980).
[10] J. M. Flesseles, A. J. Simon, and A. J. Libchaber, Adv. Phys. **40**, 1 (1991).
[11] P. G. Saffman and G. I. Taylor, Proc. R. Soc. London, Ser. A **245**, 312 (1958).
[12] For a similar dependence of spacing between fingers on growth velocity in eutectic growth, see V. Seetharaman and R. Trivedi, Metall. Trans. A **19**, 2956 (1988).
[13] J.-P. Eckmann (private communication).
[14] G. I. Sivashinsky, Annu. Rev. Fluid Mech. **15**, 179 (1983).
[15] P. Pelce and P. Clavin, J. Fluid Mech. **124**, 219 (1982).
[16] S. Smithells and K. Ingle, J. Chem. Soc. **61**, 204 (1882).
[17] M. Gorman, M. el-Hamdi, B. Pearson, and K. A. Robins, Phys. Rev. Lett. **76**, 228 (1996).
[18] J. de-Ris, *Proceedings of the 12th Symposium on Combustion* (The Combustion Institute, Pittsburgh, 1969).
[19] A. E. Frey and J. S. T'ien, Combust. Flame **36**, 263 (1979).
[20] A. E. Frey and J. S. T'ien, Combust. Flame **26**, 257 (1976).
[21] Y. Zhang, P. D. Ronney, E. V. Roegner, and J. B. Greenberg, Combust. Flame **90**, 71 (1992).
[22] A. P. Aldushin and B. J. Matkowsky, Combust. Sci. Technol. **133**, 293 (1998).
[23] A. C. Fernandez-Pello, B. J. Matkowsky, D. A. Schult, and V. A. Volpert, Combust. Flame **101**, 471 (1995).
[24] T. Kashiwagi and S. L. Olson, Proceeding of USMP-3 (National Academy of Science, Washington, DC, 1997).
[25] For the definition of Pe, see L. D. Landau and E. M. Lifshitz, *Fluid Mechanics* 209 (Pergmanon Press, London, 1976). For a discussion on the role of Pe in smoldering, see J. Buckmaster, IMA J. Appl. Math. **56**, 87 (1996).
[26] O. Zik and E. Moses, Phys. Rev. E **53**, 1760 (1995).
[27] O. Zik, Physica A **224**, 338 (1996).
[28] O. Zik, T. Kustanovich, E. Moses, and Z. Olami, Phys. Rev. E **58**, 689 (1998).
[29] The Micro Analysis Laboratory, the Hebrew University, Givat Ram, Jerusalem, Israel.
[30] *CRC Handbook of Chemistry and Physics*, 73rd ed., edited by

D. R. Lide (CRC Press, Boca Raton, 1993).
[31] We expect Pe_c, as well as the characteristic length w, to be explicitly given by a linear stability analysis of the onset regime (which must include an analysis of the heat transport).
[32] V. Fleury, J. H. Kaufman, and D. B. Hilbert, Nature (London) **367**, 435 (1994).
[33] A. Kuhn and F. Argoul, Phys. Rev. E **49**, 4298 (1994).
[34] M. Kardar, G. Parisi, and Y.-C. Zhang, Phys. Rev. Lett. **56**, 889 (1986).
[35] O. Zik, E. Moses, Z. Olami, and I. Webman, Europhys. Lett. **38**, 509 (1997).
[36] J. Zhang, Y. C. Zhang, P. Alstrom, and M. T. Levinson, Physica A **189**, 383 (1992).